ELSEVIER

Interfacial nanofabrication strategies in development of new functional nanomaterials and planar supramolecular nanostructures for nanoelectronics and nanotechnology

G.B. Khomutov[a,*], V.V. Kislov[b], M.N. Antipina[a], R.V. Gainutdinov[c], S.P. Gubin[d], A.Yu. Obydenov[a], S.A. Pavlov[a], A.A. Rakhnyanskaya[e], A.N. Sergeev-Cherenkov[a], E.S. Soldatov[a], D.B. Suyatin[a], A.L. Tolstikhina[c], A.S. Trifonov[a], T.V. Yurova[a]

[a]*Faculty of Physics, Moscow State University, Vorobjevy Gory, 119992 Moscow, Russia*
[b]*Institute of Radioengineering and Electronics RAS, 101999 Moscow, Russia*
[c]*Institute of Crystallography RAS,119899 Moscow, Russia*
[d]*Institute of General and Inorganic Chemistry RAS, 119899 Moscow, Russia*
[e]*Department of Chemistry, Moscow State University, 119992 Moscow, Russia*

Abstract

Clusters, nanoparticles, nanowires, long molecules as nanotubes and polynucleotides, and functional supramolecular nanostructures are currently considered as potential building blocks for nanotechnology and nanoelectronic devices and circuits, and development and introduction of new methods to control effectively their structure, composition and nanoscale organization are necessary. Here we describe a number of new nanofabrication methods which are based on the monolayer techniques, biomimetic principles, interfacial reactions and interactions. The methods allowed to produce new stable reproducible planar one-dimensional and two-dimensional arrays of ligand-stabilized nanoclusters and nanoparticles on solid substrates, ultrathin polymeric nanoscale-ordered mono- and multilayer quasi-crystalline and nanocomposite films, planar polymeric complex films with integrated DNA and inorganic building blocks as semiconductor and iron oxide nanoparticle quasi-linear arrays and nanowires. Transmission electron microscopy, STM and AFM techniques were used to characterize the fabricated nanostructures. Effects related to discrete electron tunneling were observed in the monolayers of nanoclusters and small gold nanoparticles at room temperature using STM.
© 2003 Elsevier B.V. All rights reserved.

Keywords: Nanoclusters; Nanoparticles; Monolayer; Ultrathin polymeric films; Electron transport

1. Introduction

Future progress in electronics will be determined by developing of more productive and compact integrated circuits and nanometer-size devices with reasonably acceptable costs. One way of advancement in electronic nanomanufacturing is based on the transformative (top-down) approach concerned with further decrease in sizes of conventional circuit elements via developments in lithography and semiconductor miniaturized processing techniques. In the other synthetic (bottom-up) approach the functional elements are proposed to be formed starting with atoms and molecules via cost-effective nanoscale-

*Corresponding author. Tel.: +7-95-939-3007; fax: +7-95-939-1195.
E-mail address: gbk@phys.msu.ru (G.B. Khomutov).

controlled assembly and self-organization processes. Clusters, nanoparticles, nanowires, long molecules as nanotubes and polynucleotides, and supramolecular nanostructures are currently considered as functional building blocks in the last approach, and the development and introduction of new methods to control effectively their structure, composition and purposeful nanoscale organization are necessary [1–3]. New interdisciplinary ideas and methods can be effective and physical-chemical techniques based on self-assembling and self-organization principles are useful for fabrication of new nanomaterials and nanostructures. It could prove that new perspective technological solutions in nanoelectronics and nanotechnology to be found on the way of building up of hybrid constructions in which advantages of both approaches are combined effectively.

Nanomaterials are expected to exhibit novel and significantly improved physical, chemical and other properties, as well as to offer opportunities for manifestation of new phenomena and processes which, owing to the nanoscale dimensions, are not observed at the macroscopic level. Thus, nanostructures are expected to present electronic conductive properties that differ considerably from those of bulk conductors: quantum resistance, ballistic transport, electron tunneling and Coulomb blockade effects [4–6]. Scanning probe microscopy and spectroscopy techniques proved to be a very effective tool for investigation of morphology and conductivity of nano-objects, in particularly, metallic clusters [7–9].

The design and integration of functional nanostructures into nanodevices and systems is the other principal step towards the new electronics. Metallic and semiconducting nanowires, long molecules as carbon nanotubes, structural and conducting polymers, in particularly, DNA, may play an important role in future electronic devices. Among the different long molecule candidates for molecular wires and scaffolds, carbon nanotubes and DNA have been the object of a substantial number of research [10,11]. A wide range of natural biological structures including proteins, lipid membranes and nucleic acids demonstrate remarkable properties for self-assembly, self-organization and self-replication. The application of biomolecular assembly processes and principles to formation of synthetic or hybrid functional nanostructures and nanostructured materials can be useful

for the bottom-up nanomanufacturing approach, especially taking into account that such synthetic procedures and building up of nanostructures being carried out at ambient and ecologically friendly conditions with high reproducibility of the structure and properties of the resulting nanomaterials characteristic for natural biological systems. Double-stranded DNA is a natural (or easily synthesized in a laboratory) organic polymer of about 2 nm diameter with unique recognition capabilities, physicochemical stability and mechanical rigidity what makes DNA a promising construction material for nanoscale frameworks and scaffolds [12]. Based on hybridization of DNA oligomers, gold nanoparticles were assembled to supramolecular aggregates [13]. Silver [14], gold [15] and platinum [16] metallic nanowires were fabricated via DNA templating.

The development of methods to fabricate ordered arrangements of chemically produced quantum dots is very important for future applications in nanoelectronics and nanotechnology. Earlier, we introduced a bioinspired approach based on the formation of mixed biomimetic Langmuir–Blodgett (LB) films consisting of inert amphiphile molecular matrix and guest organic ligand-stabilized metallic nanoclusters to create reproducible stable planar nanostructured films in which discrete electron transport effects were observed at room temperature using Scanning Tunneling Microscopy (STM) [17,18]. The double tunnel junction structure ''graphite substrate–nanocluster–STM tip'' was studied and corresponding single electron tunneling (SET) transistor based on a single nanocluster was demonstrated at room temperature for the first time [19,20]. The use of organic ligand-stabilized metal nanoclusters as building blocks for nanodevices has a number of advantages. Such chemically-synthesized metal–organic cluster molecules are characterized by the uniform size, structure and composition, and, as a result, by absolutely reproducible properties of individual nanoclusters what is of principal importance for potential mass production of quantum electronic devices. The stabilizing organic ligand shell prevents coalescence of clusters, determines their hydrophobic/hydrophilic properties and allows to regulate with Angstrom accuracy the inter-cluster distances in the organized arrays of clusters. Functional groups in the ligand shell can allow the purposeful immobiliza-

tion of clusters on substrate surfaces or in supramolecular systems.

Decomposition of an insoluble metal–organic precursor compound in a monolayer at the gas–liquid interface with following initiation of inorganic phase two-dimensional growth processes in the plain of a monolayer on the liquid surface is a basic idea of a novel approach to fabrication of inorganic nanostructures [21]. The ultimately thin and anisotropic dynamic monomolecular reaction system was realized by that method with the specific character of two-dimensional growth on the liquid surface without interaction of nucleus and growing nanoparticles with a solid substrate surface what allowed the obtaining of inorganic nanostructures with novel and unique morphologies [21,22].

In this work we present our results on the development of synthetic nanomanufacturing methods based on the interfacial nanofabrication strategies which allowed us to form ordered stable reproducible planar arrays of nanoclusters and nanoparticles on solid substrates, ultrathin polymeric nanoscale-ordered quasi-crystalline and nanocomposite films, and controlled-morphology planar polymeric complexes with DNA molecules. The monolayer and multilayer DNA/polycation complex LB films were used as templates and nanoreactors for generation of inorganic nanostructures. As a result, planar polymeric complex films with integrated DNA and inorganic building blocks as semiconductor and iron oxide nanoparticle quasi-linear arrays and nanowires were formed. The obtained nanostructures were characterized by scanning probe microscopy and transmission electron microscopy (TEM) techniques. Effects related to discrete electron tunneling were observed in the monolayer structures of ligand-stabilized nanoclusters and small gold nanoparticles at room temperature using STM.

2. Experimental

Stearic acid (SA), arachidic acid (AA), $CdCl_2$, $FeCl_3$ and salmon thimus native DNA (sodium salt) were obtained from Sigma and used as supplied. Metal–organic nanocluster molecules $1,7-(CH_3)_2-1,2C_2B_{10}H_9Tl(OCOCF_3)_2$, $Pt_5(CO)_6[P(C_6H_5)_3]_4$ and water-insoluble precursor compound for interfa-cial generation of gold nanoparticles $Au[P(C_6H_5)_3]Cl$ were synthesized in accordance with known procedures [23]. Amphiphilic polycation poly-4-vinilpyridine with 16% cetylpyridinium groups (PVP-16) was synthesized via the known conventional method [24]. PVP with polymerization degree 1100 was prepared and then quaterenized with cetyl bromide. Polymer composition was determined by IR spectroscopy measurements. Positive charges in PVP-16 molecules at neutral pH values are due to the quaternary ammonium groups, what in combination with hydrophobic groups of the molecule makes that polymer amphiphilic and water-insoluble. Milli-Q water purification system was used to produce water with an average resistivity of 18 MΩ cm for all experiments.

Surface pressure–monolayer area (π–A) isotherm measurements and monolayer deposition onto the solid substrates were carried out on a fully automatic conventional Teflon trough at 21 °C as described elsewhere [25]. Langmuir monolayers were formed by spreading a chloroform solution of amphiphilic compounds on the surface of the aqueous phase. Monolayers were transferred from the surface of aqueous subphase to the solid substrates at a constant surface pressure (π~20 mN/m), temperature (21 °C) and dipping speed (5 mm/min) using conventional vertical or horizontal substrate dipping method to form mono- and multilayer LB films. Mica substrates were used for Atomic Force Microscopy (AFM) investigations and were freshly cleaved immediately before monolayer deposition. Samples for TEM measurements were prepared by nanoparticulate monolayer deposition from aqueous subphase surface onto the Formwar film supported by the copper grid. Highly oriented pyrolytic graphite (HOPG) was used as a substrate for deposition of monolayer films for investigations by STM.

To synthesize gold nanoparticles the mixed spreading solution of $Au[P(C_6H_5)_3]Cl$ with AA in chloroform was prepared (precursor/surfactant ratio was 1:1). Spreading solution was then deposited onto the surface of aqueous phase containing sodium borohydride as a reducing agent ($NaBH_4$ concentration was 5×10^{-3} M) and the mixed precursor plus surfactant Langmuir monolayer was formed after fast solvent evaporation. Nanoparticles were formed in the two-dimensional gas phase of a monolayer (at

very low or no surface pressure), incubation time 30 min. The compression of a monolayer with grown nanoparticles to the monolayer condensed state and following deposition onto the solid substrate stopped the diffusion-mediated processes in the monolayer and fixed effectively the grown nanoparticles.

Iron oxide nanoparticles (pilot analysis pointed to maggemite and magnetite) were generated via incubation of corresponding precursor film containing Fe^{3+} cations (ferric arachidate LB film and DNA/ Fe^{3+}/PVP-16 complex film) in the sodium borohydride (10^{-4} M) or ascorbic acid (10^{-3} M) solutions followed by the film incubation in alkaline aqueous media (pH 10) at ambient conditions for 1 or 2 h. Ferric arachidate LB films were formed by the vertical lifting deposition of arachidic acid Langmuir monolayer from the surface of $FeCl_3$ solution (2×10^{-4} M, pH 2.5) onto the solid substrate surface. DNA/Fe^{3+}/PVP-16 complex film was formed via the incubation of DNA/PVP-16 complex LB film in the $FeCl_3$ solution (2×10^{-4} M, pH 2.5) for 1 h.

CdS nanoparticles and nanowires were synthesized via incubation of corresponding precursor film containing Cd^{2+} cations (DNA/Cd^{2+}/PVP-16 complex film) in the H_2S atmosphere for 2 h. DNA/Cd^{2+}/PVP-16 complex film was formed via the incubation of DNA/PVP-16 complex LB film in the $CdCl_2$ solution (2×10^{-4} M, pH 6.0) for 1 h.

STM topographic images were obtained using modified Nanoscop STM device (Digital Instruments) at ambient conditions. The images were stable and reproducible. Single nanocluster molecules and gold nanoparticles were studied spectros-copically by recording tunneling current–bias voltage (I–V) curves in a double barrier tunnel junction geometry at 21 °C, where the molecule or nanoparticle was coupled via two tunnel junctions to the two macroscopic electrodes (HOPG substrate and the tip of STM device).

AFM measurements were performed with the use of Solver P47-SPM-MDT scanning probe microscope (NT MDT, Moscow, Russia) in a tapping mode. Silicon cantilevers NSC11 (Estonia, Mikromasch) with tip-radii of about 10 nm were used. Images were measured in air at ambient temperature (21 °C) and were stable and reproducible.

TEM images of nanoparticles synthesized in Langmuir monolayer were obtained with the use of Jeol JEM-100B microscope.

3. Results and discussion

Fig. 1a shows the STM top view topographic image of 1,7-$(CH_3)_2$-1,2$C_2B_{10}H_9Tl(OCOCF_3)_2$ nanocluster molecule monolayer deposited onto the surface of HOPG substrate. One can see the compact ordered two-dimensional arrangement of nanoclusters in the monolayer with lattice parameters: $a=$ 28.0±4.0, $b=$20.0±4.0 Å, $\alpha=70°$. Image (b) in Fig. 1 represents the group of individually localized $Pt_5(CO)_6[P(C_6H_5)_3]_4$ clusters in a mixed monolayer composed by nanocluster and SA molecules with stoichiometric ratio 1:80. Highly-ordered multilayer structures of such clusters can also be formed by LB technique [26]. The two-dimensional monolayer system of metal–organic precursor molecules and
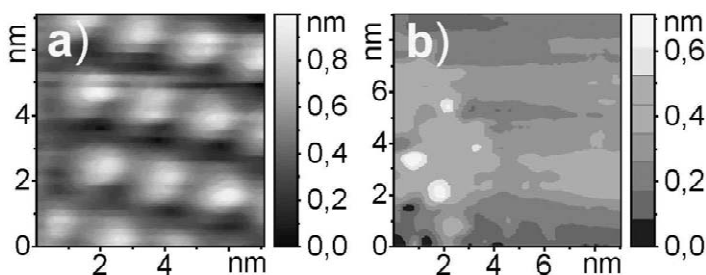

Fig. 1. STM top view topographic images of monolayers of ligand-stabilized nanoclusters deposited by horizontal substrate lifting method onto the surface of HOPG substrate (black-to-white vertical color scale is 0–1 nm). Image (a): two-dimensional closely-packed array of 1,7-$(CH_3)_2$-1,2$C_2B_{10}H_9Tl(OCOCF_3)_2$ clusters. Image (b): group of individually localized $Pt_5(CO)_6[P(C_6H_5)_3]_4$ clusters in a mixed monolayer composed by nanocluster and stearic acid molecules with stoichiometric ratio 1:80. Temperature 21 °C.
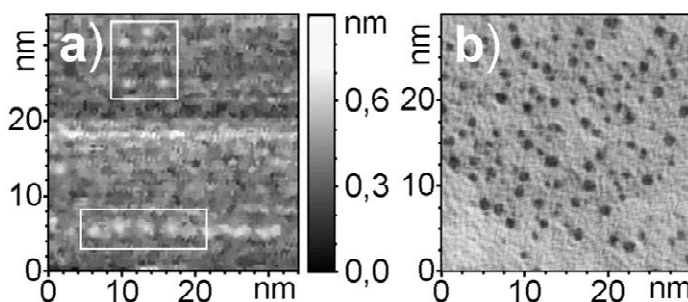
Fig. 2. Image (a): STM top view topographic image of two-dimensionally grown Au nanoparticles deposited by horizontal substrate lifting method onto the surface of HOPG substrate (black-to-white vertical color scale is 1 nm). Two areas with clearly seen nanoparticles are marked by the white frames. Au nanoparticles were synthesized in a mixed arachidic acid Langmuir monolayer (initial $Au[P(C_6H_5)_3]Cl/AA$ ratio was 1:5) on the aqueous sodium borohydride solution (5×10^{-3} M $NaBH_4$) surface at $\pi = 0$. Image (b): transmission electron micrograph showing those nanoparticles deposited onto the copper grid with Formwar coating.

surfactants on the liquid surface is a principal point in a novel approach to generation of inorganic nanostructures [21]. In that method noble metal nanoparticles can be generated by reduction of interfacially organized monolayer of insoluble pre-cursors by the reductant from the aqueous phase [22]. Gold nanoparticles synthesized using that meth-od in the mixed monolayer with AA on the surface of sodium borohydride solution are presented in Fig. 2. STM topographic image with two areas marked by the white frames where arrays of nanoparticles are easily observable is shown in Fig. 2a. Fig. 2b shows the corresponding TEM micrograph of obtained nanoparticles. The selected area electron diffraction analysis of nanoparticles synthesized by that method

indicated to the polycrystalline gold present in the sample [21]. The main diameter of the synthesized Au nanoparticles was as small as about 1.8 nm what allowed the observation of the SET effects with those nanoparticles at room temperature using STM.

Fig. 3a shows a characteristic I–V curve obtained in the double tunnel junction configuration STM tip-gold nanoparticle-conducting HOPG substrate. That I–V curve is rather symmetric and has a low conductivity gap around zero bias voltage along with the step-like periodical features with main period 290 mV. Such a shape of the I–V curve corresponds to the pure Coulomb SET process in the double tunnel junction system [6]. Coulomb staircase charging can be observed when Coulomb charging energy ($E_c =$
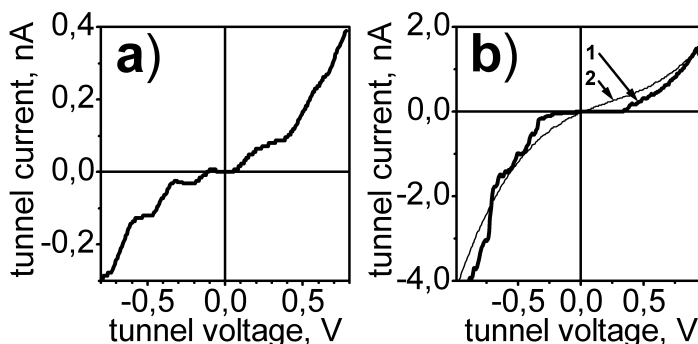

Fig. 3. Picture (a): STM tunnel current–bias voltage (I–V) dependence in the double tunnel junction configuration STM tip-gold nanoparticle-conducting HOPG substrate. Picture (b): curve 1: STM tunnel current–bias voltage (I–V) dependence in the double tunnel junction configuration STM tip—$Pt_5(CO)_6[P(C_6H_5)_3]_4$ cluster molecule—conducting HOPG substrate measured at the point above the cluster molecule. Curve 2: typical I–V curve recorded at the flat graphite substrate surface areas without cluster molecules. Temperature 21 °C.

$e^2/2C$) substantially exceeds thermal energy, k_BT, where k_B is Boltzmann's constant and T temperature ($k_BT \approx 25$ mV at room temperature) [6]. If the junction capacity C is constant the consecutive charging steps should occur at a regular spacing $\Delta V_c = e/2C$, where C is the capacitance of the junction with higher resistance. Taking the staircase period of $\Delta V_c \sim 290$ mV from Fig. 3a) we can calculate the capacitance $C = e/2\Delta V_c = 2.7 \times 10^{-19}$ F. In a classical approach, the capacitance of a conductor–insulator–spherical conducting particle junction is given by [27]:

$$C = 4\pi\varepsilon\varepsilon_0 r(1 + r/2L)$$

where ε_0 is the vacuum permittivity constant, ε is the dielectric constant of the insulator, r is the particle radius, L is the junction thickness. The isolated conducting sphere of the diameter $d = 2$ nm has capacitance $C = \varepsilon \times 1.1 \times 10^{-19}$ F. The experimental capacitance of 2.7×10^{-19} F can be reasonably well explained if we assume the effective dielectric constant $\varepsilon \sim 1.5$–2 (related to ligand, surfactant and adsorbate layers) and take into account the capacitance increase due to the geometric factors of the real junction configuration. Similar Coulomb charging effects were observed at room temperature with nano-sized gold [9,28–30] and Co [31] nanoparticles. Single-electron charging effects were also observed at room temperature in a planar multilayer system—metal electrode–insulator–gold nanoparticle–insulator–metal electrode formed by the layer-by-layer stepwise assembly technique [32]. A characteristic I–V curve measured in the double tunnel junction configuration STM tip–$Pt_5(CO)_6[P(C_6H_5)_3]_4$ cluster–conducting HOPG substrate is presented in Fig. 3b (curve 1) and has a number of similar and different features in comparison with the I–V curve in Fig. 3a. First, the suppressed conductivity area at low bias voltage amplitudes (~360 mV) is clearly seen in Fig. 3b, curve 1. Second, that curve is asymmetrical and exhibits steps-like features with variable widths and heights. The shape details of the I–V curves recorded above the nanocluster can depend on the STM settings, but the aforementioned characteristic features were present in all I–V curves independently of the current recording from negative to positive bias

voltages or vice versa [2]. For comparison, curve 2 in Fig. 3b shows a typical I–V curve without such features recorded at the flat HOPG substrate surface areas in the absence of nanoclusters. Rich structures in the nanocluster I–V characteristics indicate to the complex character of electron tunneling through the nanocluster molecule with probable manifestation of sequential discrete electron tunneling effects resulting from a number of factors as high tunnel resistivity of the system and interplay between Coulomb charging effects, resonant tunneling through discrete states of electrons in the nanocluster, electronic–vibrational coupling in the molecular system. Also, micromechanical vibration effects were assumed to play a role in the electron transport in such nanocluster supramolecular systems [33]. The higher value of suppressed conductance gap voltage (~360 mV) on curve 1 of Fig. 3b obtained for the $Pt_5(CO)_6[P(C_6H_5)_3]_4$ cluster can be due to the smaller metallic core diameter of the cluster and, as a result, smaller effective junction capacity. Also, the cluster HOMO–LUMO gap can have an effect upon the electron transport in that tunnel system. Similar complex electron tunneling effects were observed in STM spectroscopic studies of isolated fullerene molecules [34] and cytochrome c molecules [35] giving evidence for the similar sequential discrete electron tunneling mechanisms in such immobilized metalloprotein and nanocluster structures which can be of interest for development of bioelectronic and hybrid functional nanoelectronic systems with biological redox components integrated into synthetic structures or vice versa.

The appropriate design, rational assembling and integration of nanoscale functional building blocks into one-, two- and three-dimensional architectures are the principal steps on the way to fundamental scientific understanding of their individual and collective optical, electronic, magnetic and other properties which is necessary for real advancements of nanomaterials to technologically important applications. To fabricate ordered planar quasi-one-dimensional arrays of chemically produced quantum dots (clusters and nanoparticles) we have proposed an approach schematically described in Fig. 4. In this approach the polymeric smectic liquid crystal-like planar monolayer structure of amphiphilic polycation molecules is formed on the surface of a liquid phase
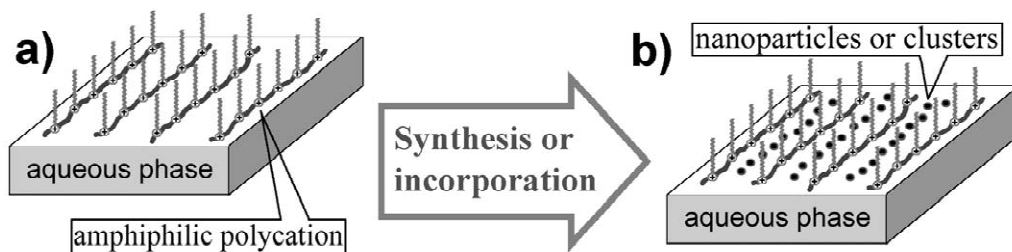
Fig. 4. Schematic diagram of the polymeric smectic liquid crystal planar monomolecular structure formed at the gas–liquid interface using amphiphilic polyelectrolyte molecules (a), and corresponding nanoscale-ordered composite planar polymeric structure with incorporated functional nanoscopic components—nanoclusters or nanoparticles (b).

and serves as an organizing stable monomolecular media. Then, polymeric nanoscale-ordered nanocomposite film can be formed via the incorporation of previously prepared inorganic or organic functional components in the polymeric monolayer or via the interfacial synthesis directly in the monolayer. Further deposition of such a monolayer onto the solid substrates allows fabrication of organized ultrathin mono- and multilayer quasi-crystalline composite polymeric films and coatings. Such quasi-crystalline polymeric films with thickness down to a monolayer can be of use for nanotechnological applications because different functional nano-size

elements (as guest molecules; ligand-stabilized nanoclusters; metallic, oxidic or semiconducting nanoparticles, nanocrystals, nanorods and nanowires, etc.) can be incorporated in such films to form ultimately thin highly-ordered planar composite polymeric nanostructures which are hardly available with other techniques. That approach is potentially compatible with a wide range of planar technologies which are or will be used for fabrication of nanodevices.

Fig. 5 demonstrates the AFM tapping mode top view topographic image of PVP-16 two-layer LB film on the mica substrate. One can see the ordered
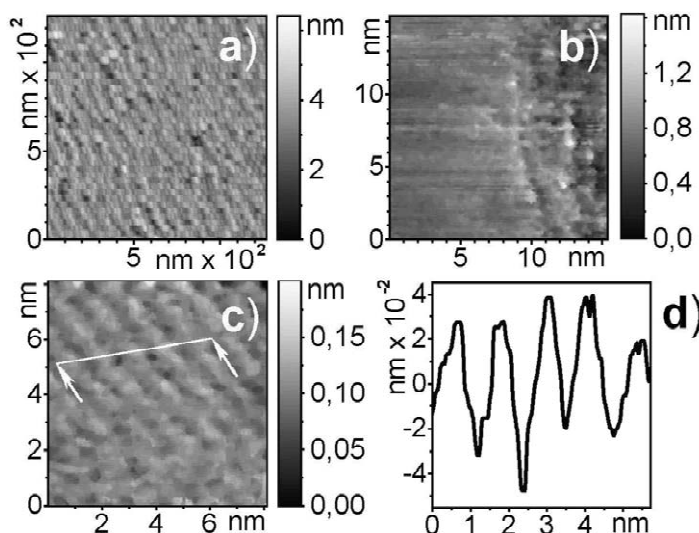

Fig. 5. Image (a): AFM tapping mode top view topographic image of PVP-16 two-layer LB film on the mica substrate. Images (b) and (c): STM top view topographic images of composite PVP-16 monolayer with incorporated $Pt_5(CO)_6[P(C_6H_5)_3]_4$ cluster molecules. Monolayer was deposited by horizontal substrate lifting method onto the surface of HOPG substrate. Image (d): characteristic cross-section profile of image (c) marked by the arrows.

fine structure of the film with grains of ~40 nm due to the surface micelle formation. The tendency for linear parallel chain-like organization of surface micelles in PVP-16 LB films can be a result of smectic liquid crystal-like ordering of linear PVP-16 molecules on the aqueous phase surface. In the thermodynamically equilibrium state of the monolayer the positively charged PVP-16 molecules have to be organized as planar quasi-parallel string-like structures (two-dimensional smectic liquid crystal) due to the electrostatic repulsive intramolecular interaction between the charged links and inter-molecular repulsion of charged extended linear poly-cation molecules. Images (b) and (c) in Fig. 5 show STM top view topographic images of composite PVP-16 monolayer with incorporated $Pt_5(CO)_6[P(C_6H_5)_3]_4$ cluster molecules deposited on the HOPG substrate. The quasi-one-dimensional chain structures of clusters are visible on those images. The characteristic cross-section profile of

image (c) is presented in picture 5d and demonstrates the topographic features in the film with characteris-tic size ~1.2 nm which is close to the size of the cluster molecule [2].

Fig. 6 represents the characteristic AFM topog-raphic images of the deposited DNA/PVP-16 com-plex films on atomically-flat mica substrate. Fig. 6a represents the characteristic AFM topographic image of the deposited DNA/PVP-16 complex in which bound DNA molecules form complex planar net-like or lattice structures. The specific feature of the DNA/PVP-16 complex formation in that experiment was the DNA interaction with uncompressed mono-layer of amphiphilic polycation at low ionic strength (1 mM NaCl). In such a monolayer PVP-16 mole-cules are at the maximal distance from each other due to the electrostatic repulsive interactions and entropic factor and form rarefied two-dimensional gaseous phase of the monolayer with rather low surface concentration of PVP-16 molecules. The
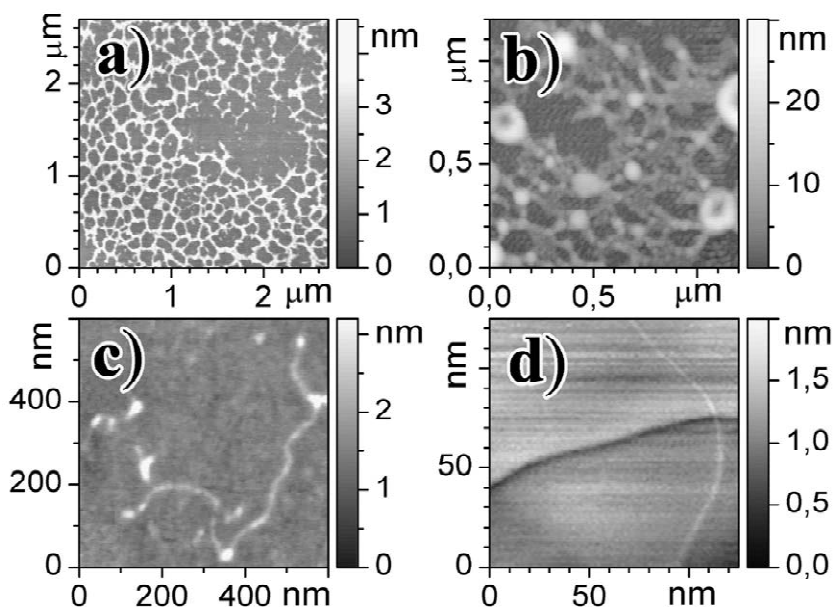

Fig. 6. Image (a): AFM tapping mode top view topographic image of DNA/PVP-16 complex two-layer LB film on the mica substrate. Complex formation conditions: PVP-16 monolayer surface pressure value ~0 during the DNA binding, incubation time 25 min. The composition of the aqueous subphase was 1.2×10^{-4} M DNA (for monomer), 1 mM NaCl, pH 6. Image (b): AFM tapping mode top view image of DNA/PVP-16 complex two-layer LB film on the mica substrate. Complex formation conditions: PVP-16 monolayer surface pressure value 20 mN/m during the DNA binding, incubation time 25 min. The same composition of the aqueous subphase as on image (a). Image (c): AFM tapping mode top view image of individual DNA molecule observed in DNA/PVP-16 complex two-layer LB film on the mica substrate. Image (d): STM top view topographic image of individual DNA molecule observed in DNA/PVP-16 complex monolayer LB film on the HOPG substrate.

anionic DNA molecules in extended coil conformation interact with individual linear extended amphiphilic polycation PVP-16 molecules at the aqueous phase/air interface, and the effective surface concentration of PVP-16 molecules interacting with DNA molecules (which are at the constant concentration in the bulk aqueous phase) can be changed and adjusted controllably via variation of the PVP-16 Langmuir monolayer area. The anionic groups in the double-stranded native DNA molecule (two phosphate groups every 3.5 Å [36]) are charged to a degree of about 0.5 negative charge per phosphate group at low ionic strength [37] which is substantially higher than the linear charge density of one positive charge per ~25 Å in the extended PVP-16 molecule. As a result, multimolecular aggregation of the stretched DNA and linear PVP-16 molecules can occur at the air–aqueous phase interface with formation of net-like or lattice structures organized as interconnected DNA/PVP-16 complexes with extended conformations. Single stretched DNA molecules bound with PVP-16 monolayer were also observed (Fig. 6c and d). In the case of compressed PVP-16 monolayer the linear DNA molecules from the bulk aqueous phase interact with organized positively charged surface of the compressed compact cationic PVP-16 monolayer with maximal effective surface concentration of PVP-16 molecules and there is no such anisotropy in the arrangement of surface positive charges as in the first case of uncompressed amphiphilic polycation monolayer. The structure of resulting PVP-16/DNA planar complex in that case is presented in Fig. 6b and is different substantially from that shown in Fig. 6a. Coexisting planar quasi-circular compact toroidal and linear structures are clearly seen in Fig. 6b. The outer diameters for toroidal condensates varied between 30 and 300 nm. Also, the fine structure of ordered arrays of surface micelles in PVP-16 monolayer (similar to that in Fig. 5a) is clearly seen in Fig. 6b giving evidence for the undisturbed compact ordered structure of the compressed PVP-16 monolayer in that interfacial DNA/PVP-16 complex. Formation of the circular structures obtained when DNA interacted with compressed PVP-16 monolayer can be understood as DNA compactization with formation of toroidal structures typically observed when DNA was condensed via electrostatic interac-

tions with cationic compounds (polyamines, peptides, cationic surfactants and metal cations) or via changing the water activity in the microenvironment of DNA molecule by alcohols [38,39]. Similar toroidal and linear morphologies were typically observed for bulk phase DNA condensates with cationic polymers [40].

The obtained planar DNA-based self-organized polymeric complex nanostructures can prove to be a promising construction material for nanoscale frameworks and scaffolds in the fabrication of nanodevices. Here we demonstrate the use of these DNA/polycation complex LB films as organized templates and nanoreactors for generation of inorganic nanostructures. Fig. 7 shows the characteristic TEM micrographs with iron oxide nanoparticles formed in the ferric arachidate LB film (image 7a), iron oxide (images 7b and 7c) and CdS (image d) nanoparticles and nanowires grown in the planar supramolecular nanoreactors—DNA/metal cation/PVP-16 complex films. Randomly distributed iron oxide nanoparticles with main diameter about 5 nm were grown in the ferric arachidate LB film (Fig. 7a). Ordered quasi-linear arrays of small iron oxide nanoparticles (main diameter~2,5 nm) were obtained in DNA/PVP-16 complex film (Fig. 7b) giving evidence for important spatial organizing role of DNA and polycation molecules in those nanocomposite structures. The difference in size of iron oxide nanoparticles in Fig. 7a and b can be a result of smaller quantity of initial Fe^{3+} cations in the precursor DNA/Fe^{3+}/PVP-16 complex LB film in comparison with ferric arachidate LB film, and also can reflect the differences in the interactions of growing nanoparticles with stabilizing and immobilizing organic ligand groups in those films. Also, iron oxide and CdS nanowires (diameter about 5 nm) were obtained (images 7c and 7d, correspondingly). Aggregation and intergrowth of linearly-organized nanoparticles in such polymeric complex nanoreactor can be a mechanism of nanowire formation.

4. Conclusions

A number of new synthetic and assembling nanofabrication methods based on the surface and
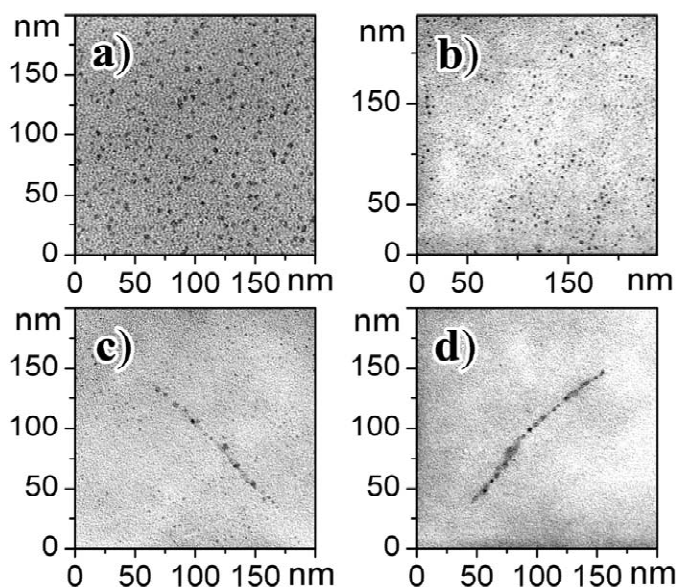
Fig. 7. Transmission electron micrographs showing iron oxide and CdS nanoparticles and nanostructures grown in planar supramolecular nanoreactors. Image (a): iron oxide nanoparticles generated in ferric arachidate LB film (incubation 1 h). Image (b): iron oxide nanoparticles synthesized in $DNA/Fe^{3+}/PVP$-16 complex LB film (incubation time 1 h). Image (c): iron oxide nanoparticles and nanowire synthesized in $DNA/Fe^{3+}/PVP$-16 complex LB film (incubation time 2 h). Image (d): CdS nanowire synthesized in $DNA/Cd^{2+}/PVP$-16 complex LB film.

interface interactions have been developed. Stable planar supramolecular nanostructures with ligand-stabilized metallic nanoclusters and small gold nanoparticles were fabricated by the liquid–gas interface monolayer approach. Discrete electron tunneling effects were observed in such structures at room temperature using STM which open perspectives for applications of those structures in research and development of nanoelectronic elements and devices based on the controlled SET effects. Polymeric smectic liquid quasi-crystal planar monomolecular structures were formed at the gas–liquid interface using amphiphilic polyelectrolyte, and corresponding nanoscale-ordered composite planar polymeric films with incorporated ligand-stabilized metal clusters were fabricated successfully for the first time. Effects of two-dimensional nanoscale supramolecular organization and patterning were observed in the interface monolayer amphiphilic polycation/DNA complexes dependent on the cationic amphiphile monolayer state during the DNA binding. Planar polymeric complex films with integrated DNA and inorganic building blocks as semiconductor (CdS) and iron oxide nanoparticle quasi-linear arrays and nanowires were formed successfully. The data obtained give evidence for the effectiveness of interfacial monolayer techniques to study mechanisms of structural transformations in the processes of DNA complexation with amphiphilic polycations and demonstrate its perspectives for creation of planar DNA-based self-organized polymeric complex nanostructures with nanoscale structural ordering which can be a promising construction material for nanoscale frameworks and scaffolds. The methods developed can be perspective for design and fabrication of new controlled-morphology ultimately thin highly-ordered planar composite polymeric nanostructured materials, composite films and coatings with thickness down to a monolayer for applications in nanoelectronics and nanotechnology.

Acknowledgements

References

[1] S. Roth, M. Burghard, G. Leising, Curr. Opin. Solid State Mater. Sci. 3 (1998) 209–215.

[2] S.P. Gubin, Yu.A. Gulayev, G.B. Khomutov, V.V. Kislov, V.V. Kolesov, E.S. Soldatov, K.S. Sulaimankulov, A.S. Trifonov, Nanotechnology 13 (2002) 185–194.

[3] A.P. Alivisatos, Science 271 (1996) 933–937.

[4] S. Datta, Electronic Transport in Mesoscopic Systems, Cambridge University Press, Cambridge, 1997.

[5] H. Ahmed, K. Nakazato, Microelectron. Eng. 32 (1996) 297–315.

[6] K.K. Likharev, Proc. IEEE 87 (1999) 606–632.

[7] R.H. Terrill, T.A. Postlethwaite, C.H. Chen, C.D. Poon, A. Terzis, A.D. Chen, J.E. Hutchison, M.R. Clark, G. Wignall, J.D. Londono, R. Superfine, M. Falvo, C.S. Johnson, E.T. Samulski, R.W. Murray, J. Am. Chem. Soc. 117 (1995) 12537–12541.

[8] M.T. Reetz, W. Helbig, S.A. Quaiser, U. Stimming, N. Breuer, R. Vogel, Science 262 (1995) 367–370.

[9] P.J. Durston, J. Schmidt, R.E. Palmer, J.P. Wilcoxon, Appl. Phys. Lett. 71 (20) (1997) 2940–2942.

[10] R. Saito, M.S. Dresselhaus, G. Dresselhaus (Eds.), Physical Properties of Carbon Nanotubes, Imperial College, London, 1998.

[11] C.M. Niemeyer, Curr. Opin. Chem. Biol. 4 (2000) 609–618.

[12] C.M. Niemeyer, Appl. Phys. A 68 (1999) 119–124.

[13] C.A. Mirkin, Inorg. Chem. 39 (2000) 2258–2272.

[14] J.J. Storhoff, C.A. Mirkin, Chem. Rev. 99 (1999) 1849–1862.

[15] O. Harnack, W.E. Ford, A. Yasuda, J.M. Wessels, Nanoletters 2 (2002) 919–923.

[16] M. Mertig, L.C. Ciacchi, R. Seidel, W. Pompe, Nanoletters 2 (2002) 841–844.

[17] A.A. Zubilov, S.P. Gubin, A.K. Korotkov, A.G. Nikolaev, E.S. Soldatov, V.V. Khanin, G.B. Khomutov, S.A. Yakovenko, Techn. Phys. Lett. 20 (1994) 195–201.

[18] G.B. Khomutov, E.S. Soldatov, S.P. Gubin, S.A. Yakovenko, A.S. Trifonov, A.Yu. Obydenov, V.V. Khanin, Thin Solid Films 327–329 (1998) 550–553.

[19] S.P. Gubin, V.V. Kolesov, E.S. Soldatov, A.S. Trifonov, V.V. Khanin, G.B. Khomutov, S.A. Yakovenko, Tunneling device, US Pat. 6,057,556, 2 May 2000.

[20] E.S. Soldatov, V.V. Khanin, A.S. Trifonov, S.P. Gubin, V.V. Kolesov, D.E. Presnov, S.A. Yakovenko, G.B. Khomutov, JETP Lett. 64 (1996) 556–560.

[21] G.B. Khomutov, Colloids Surfaces A 202 (2002) 243–267.

[22] G.B. Khomutov, S.P. Gubin, Mater. Sci. Eng. C 22 (2) (2002) 141–146.

[23] S.P. Gubin, Chemistry of Clusters, Nauka, Moscow, 1987.

[24] R.M. Fuoss, U.P. Strauss, J. Polym. Sci. 3 (1948) 246–253.

[25] G.B. Khomutov, S.A. Yakovenko, E.S. Soldatov, V.V. Khanin, M.D. Nedelcheva, T.V. Yurova, Membr. Cell Biol. 10 (1997) 665–677.

[26] A.Yu. Obydenov, S.P. Gubin, V.V. Khanin, S.N. Polyakov, A.N. Sergeev-Cherenkov, E.S. Soldatov, A.S. Trifonov, G.B. Khomutov, Colloid Surfaces A 198–200 (2002) 389–400.

[27] J.B. Barner, S.T. Ruggerio, Phys. Rev. Lett. 59 (1987) 807–812.

[28] D.L. Klein, P.L. McEuen, J.E.B. Katari, R. Roth, A.P. Alivisatos, Appl. Phys. Lett. 68 (1996) 2576–2580.

[29] R.P. Andres, T. Bein, M. Dorogi, S. Feng, J.I. Henderson, C.P. Kubiak, W. Mahoney, R.G. Osifchin, R. Reifenberger, Science 272 (1996) 1323–1326.

[30] G. Schmid, Y.-P. Liu, M. Schumann, T. Raschke, C. Radehaus, Nanoletters 1 (2001) 405–409.

[31] C. Petit, T. Cren, D. Roditchev, W. Sacks, J. Klein, M.-P. Pileni, Adv. Mater. 11 (1999) 1198–1203.

[32] D.L. Feldheim, K.C. Grabar, M.J. Natan, T.E. Mallouk, J. Am. Chem. Soc. 118 (1996) 7649–7651.

[33] L.Y. Gorelik, A. Isacsson, M.V. Voinova, B. Kasemo, R.I. Shekhter, M. Jonson, Phys. Rev. Lett. 80 (1998) 4526–4529.

[34] D. Porath, Y. Levi, M. Tarabiah, O. Millo, Phys. Rev. D 56 (15) (1997) 9829–9833.

[35] G.B. Khomutov, L.V. Belovolova, S.P. Gubin, V.V. Khanin, A.Yu. Obydenov, A.N. Sergeev-Cherenkov, E.S. Soldatov, A.S. Trifonov, Bioelectrochemistry 55 (2002) 177–181.

[36] A.L. Lehninger, Biochemistry, Worth Publishers, New York, 1972.

[37] D. Stigter, Biophys. J. 69 (1995) 380–388.

[38] V.A. Bloomfield, Curr. Opin. Struct. Biol. 6 (1996) 334–341.

[39] T.H. Eickbush, E.N. Moudrianakis, Cell 13 (1978) 295–306.

[40] B.J. Rackstraw, A.L. Martin, S. Stolnik, C.J. Roberts, M.C. Garnett, M.C. Davies, S.J.B. Tendler, Langmuir 17 (2001) 3185–3193.